International Communications in Heat and Mass Transfer 37 (2010) 695–702

Contents lists available at ScienceDirect

International Communications in Heat and Mass Transfer

journal homepage: www.elsevier.com/locate/ichmt

Slip-flow and heat transfer of gaseous flows in the entrance of a wavy microchannel ☆

H. Shokouhmand, S. Bigham *

School of Mechanical Engineering, College of Engineering, University of Tehran, Tehran, Iran

ARTICLE INFO

Available online 9 April 2010

Keywords:
Microchannel
Wavy geometry
Slip boundary condition

ABSTRACT

The present work investigates the developing fluid flow and heat transfer through a wavy microchannel with numerical methods. Governing equations including continuity, momentum and energy with the velocity slip and temperature jump conditions at the solid walls are discretized using the finite-volume method and solved by SIMPLE algorithm in curvilinear coordinate. The effects of creep flow and viscous dissipation are assumed. The numerical results are obtained for various Knudsen numbers. The results show that Knudsen number has declining effect on both the C_f.Re and Nusselt number on the undeveloped fluid flow. Significant viscous dissipation effects have been observed for large Knudsen number. Also, viscous dissipation causes a singular point in Nusselt profiles.

1. Introduction

The study of fluid behavior in devices with micro-scale geometries has received many interests because of its extensive applications in micro-electro-mechanical-systems (MEMS), microelectronics cooling, micro-scale heat exchangers, reactors, power systems, drug delivery and biotechnical analyses.

A typical geometry of the flow passage that is used for enhancing the rate of heat and mass transfer is wavy wall channel. However, there are a few experimental and numerical investigations available to give a clear understanding of convective heat transfer rates and hydrodynamic characteristics of gaseous flows in the slip flow regime through wavy microchannels. Therefore, an accurate and efficient analysis of hydrodynamic and thermal behavior of gaseous flows in wavy microchannels seems necessary.

One of the important challenges associated with the computational analysis of micro-scale gaseous flows originates from the fact that the flow physics tend to get changed altogether, as one reduces the length scales from the macro domain to the micro domain. Due to the reduced length scale of micro-scale devices, the transfer lengths are short and the areas are small, but high surface-to-volume ratios and tiny volumes dominate everything and cause different behaviors in comparison with macro-scale channels. The rarefaction effect is one of the important effects in micro-scale geometries. The Knudsen number is a measure of the degree of rarefaction, which is defined as the ratio of the mean free path to the appropriate macroscopic length scale of the flow. As the value of Knudsen number increases, rarefaction effects become more important and thus pressure drop, shear stress, heat flux, and corresponding mass flow rate cannot be predicted from flow and heat transfer based on the continuum hypothesis. For Knudsen numbers in the range $10^{-3} \leq Kn \leq 10^{-1}$, molecular collisions with the walls dominate over intermolecular collisions. This thin layer is called the Knudsen layer and the flow regime in this range of Knudsen numbers is known as slip-flow regime. In slip-flow regime the standard Navier–Stokes and energy equations can still be used with modifications to the boundary conditions allowing for velocity slip and temperature jump at the walls [1–3].

In the past decade, considerable efforts have been devoted to analyze fluid flow and heat transfer in wavy channel and microchannel. Wang et al. [4] numerically studied forced convection in a symmetric wavy wall macrochannel. They reported the effects of the wavy geometry, Reynolds number and Prandtl number on the skin-friction and Nusselt number. O'Brien and Sparrow [5] studied the heat transfer characteristics in the fully developed region of a periodic channel in the Reynolds number range of Re = 1500 to Re = 25000. A level of heat transfer enhancement by about a factor of 2.5 over a conventional straight channel was observed, resulting from a highly complex flow pattern including a strong forward flow and an oppositely directed recalculating flow.

Arkilic et al. [6] investigated helium flow through microchannels. It is found that the pressure drop over the channel length was less than the continuum flow results. The friction coefficient was only about 40% of the theoretical values. Beskok et al. [7] studied the rarefaction and compressibility effects in gas microflows in the slip flow regime and for the Knudsen number below 0.3. Their formulation is based on the classical Maxwell/Smoluchowski boundary conditions that allow partial slip at the wall. It was shown that rarefaction negates

☆ Communicated by W.J. Minkowycz.

* Corresponding author.
E-mail addresses: sajjadbigham@ut.ac.ir, sajjadbigham@gmail.com (S. Bigham).

0735-1933/$ – see front matter © 2010 Elsevier Ltd. All rights reserved.
doi:10.1016/j.icheatmasstransfer.2010.03.008

Nomenclature

a	amplitude of the wave (m)
k	thermal conductivity of air (W/m K)
h	local heat transfer coefficient (W/m^2.K)
J	Jacobian of the coordinate transformation
p	dimensionless pressure
Re	Reynolds number ($\mathrm{Re}=\rho u_i^* L^*/\mu$)
Pr	Prandtl number ($\mathrm{Pr}=\nu/\alpha$)
Nu	local Nusselt number
Nu_∞	fully developed Nusselt number
Kn	Knudsen number
Ma	Mach number
Pe	Peclet number
Ec	Eckert number
C_f	skin-friction coefficient
c_p	specific heat (J/kg K)
n	dimensionless normal direction to the wall
s	dimensionless tangential direction to the wall
q11,q22,q12	grid parameters
R	gas constant (J/kg K)
T	temperature (K)
q''	heat flux
u	dimensionless velocity component in x-direction
v	dimensionless velocity component in y-direction
L^*	channel inlet width
x	dimensionless horizontal coordinate
y	dimensionless vertical coordinate

Greek symbols

α	thermal diffusivity(m^2/s)
λ	dimensionless surface wavelength (m)
ρ	density of fluid (kg/m^3)
μ	dynamic viscosity (kg/m s)
γ	ratio of specific heats (c_p/c_v)
λ	molecular mean free path (m)
ν	kinematic viscosity(m^2/s)
σ_T	energy accommodation coefficient
σ_v	momentum accommodation coefficient
θ	dimensionless temperature
ξ	curvilinear horizontal coordinate
η	curvilinear vertical coordinate
τ	shear stress

Subscripts

ave	mean value
w	surface conditions
i	inlet conditions
s	fluid property near the wall

Superscripts

C	contravariant velocities
tang	tangential direction
*	returns to dimensional parameters

compressibility. They also suggested specific pressure distribution and mass flow rate measurements in microchannels of various cross sections. Kuddusi et al. [8] studied the thermal and hydrodynamic characters of a hydrodynamically developed and thermally developing flow in trapezoidal silicon microchannels. It was found that the friction factor decreases if rarefaction and/or aspect ratio increase. Their work also showed that at low rarefactions the very high heat transfer rate at the entrance diminishes rapidly as the thermally developing flow approaches fully developed flow. Chen et al. [9] investigated the mixing characteristics of flow through microchannels with wavy surfaces. However, they modeled the wavy surface as a series of rectangular steps which seems to cause computational errors at boundary especially in micro-scale geometry. Also their working fluid was liquid and they imposed no-slip boundary conditions at the microchannel wall surface.

The review of the previous works showed that numerous studies were conducted on wavy channel in macro-scale. However, according to the authors' knowledge, there is no study of hydrodynamic and thermal characteristics of fluid flow in wavy microchannels with slip boundary conditions. The present investigation is devoted to study the developing fluid flow and heat transfer through a wavy microchannel with the velocity slip and temperature jump conditions at the solid walls.

2. Physical model and governing equations

Let us consider a rarefied gas through a symmetric wavy microchannel. The physical domain and coordinates under consideration are illustrated in Fig. 1. The mathematical non-dimensional expression of wavy wall is given as

$$y_{w,A}(x) = 0.5 + a\left(1-\sin\left(2\pi\left(\frac{x}{\lambda}-0.125\right)\right)\right)$$

Fluid flow and heat transfer are supposed to be steady, two-dimensional, laminar and incompressible. The channel walls are assumed to extend to infinity in the z-direction (i.e., perpendicular to the plane). Physical properties are assumed to be constant. The present work is concerned with both thermally and hydrodynamically developing flow cases. In this study, the usual continuum approach is coupled with two main characteristics of the micro-scale phenomena, the velocity slip and the temperature jump. A general non-orthogonal curvilinear coordinate framework with (ξ,η) as independent variables is used to formulate the problem. The non-dimensional governing equations can be written as:

Continuity:

$$\frac{\partial U^C}{\partial \xi}+\frac{\partial V^C}{\partial \eta}=0 \tag{1}$$

X-momentum:

$$\frac{\partial}{\partial \xi}\left(uU^C\right)+\frac{\partial}{\partial \eta}\left(uV^C\right)=\frac{1}{Re_i}\left\{\frac{\partial}{\partial \xi}\left(q_{11}\frac{\partial u}{\partial \xi}\right)+\frac{\partial}{\partial \eta}\left(q_{22}\frac{\partial u}{\partial \eta}\right)+\frac{\partial}{\partial \xi}\left(q_{12}\frac{\partial u}{\partial \eta}\right)+\frac{\partial}{\partial \eta}\left(q_{12}\frac{\partial u}{\partial \xi}\right)\right\}-\frac{\partial}{\partial \xi}\left(y_\eta p\right)+\frac{\partial}{\partial \eta}\left(y_\xi p\right) \tag{2}$$

Y-momentum:

$$\frac{\partial}{\partial \xi}\left(vU^C\right)+\frac{\partial}{\partial \eta}\left(vV^C\right)=\frac{1}{Re_i}\left\{\frac{\partial}{\partial \xi}\left(q_{11}\frac{\partial v}{\partial \xi}\right)+\frac{\partial}{\partial \eta}\left(q_{22}\frac{\partial v}{\partial \eta}\right)+\frac{\partial}{\partial \xi}\left(q_{12}\frac{\partial v}{\partial \eta}\right)+\frac{\partial}{\partial \eta}\left(q_{12}\frac{\partial v}{\partial \xi}\right)\right\}+\frac{\partial}{\partial \xi}\left(x_\eta p\right)-\frac{\partial}{\partial \eta}\left(x_\xi p\right) \tag{3}$$

Energy:

$$\frac{\partial}{\partial \xi}\left(\theta U^C\right)+\frac{\partial}{\partial \eta}\left(\theta V^C\right)=\frac{1}{Pe_i}\left\{\frac{\partial}{\partial \xi}\left(q_{11}\frac{\partial \theta}{\partial \xi}\right)+\frac{\partial}{\partial \eta}\left(q_{22}\frac{\partial \theta}{\partial \eta}\right)+\frac{\partial}{\partial \xi}\left(q_{12}\frac{\partial \theta}{\partial \eta}\right)+\frac{\partial}{\partial \eta}\left(q_{12}\frac{\partial \theta}{\partial \xi}\right)\right\}+\varphi \tag{4}$$

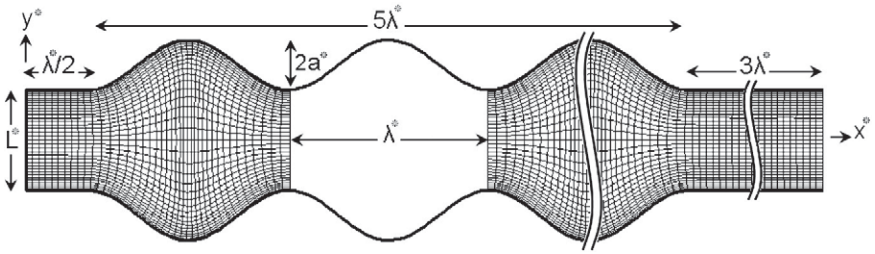

Fig. 1. The physical domain of wavy microchannel.

where:

$$V^C = -uy_\xi + vx_\xi, U^C = uy_\eta - vx_\eta, J = x_\xi y_\eta - x_\eta y_\xi,$$

$$q_{11} = \frac{1}{J}\left(y_\eta^2 + x_\eta^2\right), q_{12} = \frac{-1}{J}\left(x_\xi x_\eta + y_\xi y_\eta\right)$$

$$q_{22} = \frac{1}{J}\left(x_\xi^2 + y_\xi^2\right), \varphi = \frac{Ec_i}{\mathrm{Re}_i J}\left\{2\left(u_\xi y_\eta - u_\eta y_\xi\right)^2 + 2\left(-v_\xi x_\eta + v_\eta x_\xi\right)^2 + \left(-u_\xi x_\eta + u_\eta x_\xi + v_\xi y_\eta - v_\eta y_\xi\right)^2\right\}$$

where u, v are the velocity components and U^c and V^c are the velocities in ξ,η , respectively and Φ represents the dissipation function stems from viscous stresses. The employed dimensionless variables are defined as follows:

$$x = \frac{x^*}{L^*}, y = \frac{y^*}{L^*}, p = \frac{p^*}{\rho {u_i}^{*2}}, u = \frac{u^*}{{u_i}^*}, v = \frac{v^*}{{u_i}^*}, Re_i = \frac{\rho {u_i}^* L^*}{\mu},$$

$$Pe_i = Re_i Pr = \frac{{u_i}^* L^*}{\alpha}, \theta = \frac{T - T_i}{T_w - T_i}.$$

3. Slip flow effects and boundary conditions

When gas flows in conduits with micron scale dimensions or in low pressures conditions, a sublayer starts growing. This sublayer is on the order of one mean free path, known as the Knudsen layer, begins to become dominant between the bulk of the fluid and the wall surface. However this sublayer is small in comparison with the microchannel height for $\mathrm{Kn} \leq 0.1$ and can be ignored by extrapolating the bulk gas flow towards the walls. This causes a finite velocity slip value at the wall, and a nonzero difference between temperature of solid boundaries and the adjacent fluid. It means a slip flow and a temperature jump will be present at solid boundaries. This flow regime is known as the slip flow regime. In this flow regime, the Navier–Stokes equations are still valid together with the modified boundary conditions at the wall.

In order to calculate the slip velocity at wall under rarified condition, the Maxwell slip condition has been widely used. Maxwell supposed on a control surface, s, at a distance $\lambda/2$, half of the molecules passing through s are reflected from the wall, the other half of the molecules comes from one mean free path away from the surface with tangential velocity u_λ. On the assumption that a fraction σ_v of the molecules are reflected diffusively at the walls and the remaining $(1-\sigma_v)$ of the molecules are reflected specularly, Maxwell obtained the following expression by using Taylor expansion for u_λ about the tangential slip velocity of the gas on this surface namely u_s. Also von-Smoluchowski's temperature jump boundary conditions that is a derivation based on the kinetic theory of gases are used, [10–12]:

$$U_s = \frac{2-\sigma_v}{\sigma_v} Kn_i \left.\frac{\partial U_s}{\partial n}\right|_w + \frac{3}{2\pi}\frac{(1-\gamma)}{\gamma}\frac{Kn_i^2 Re_i}{Ec_i}\left.\frac{\partial \theta}{\partial s}\right|_w, \quad (5)$$

$$\theta_s = 1 - \left(\frac{2-\sigma_T}{\sigma_T}\right)\left(\frac{2\gamma}{\gamma+1}\right)\frac{Kn_i}{\mathrm{Pr}_i}\left.\frac{\partial \theta}{\partial n}\right|_w$$

where γ and σ represent the specific heat ratio and accommodation coefficient, respectively. The second term in the slip velocity associates with the thermal creep. The thermal creep (transpiration) phenomenon is a rarefaction effect. It shows that even without any pressure gradient, the flow can be caused due to tangential temperature gradient, specifically from colder region toward warmer region. [10–12]. Here, Ec_i means the Eckert number in inlet which is defined as

$$Ec_i = \frac{{u_i}^{*2}}{c_p (T_w - T)_i} \quad (6)$$

where Pr and Kn mean the Prandtl number and Knudsen number, respectively.

In this work we concentrate on incompressible flow. The flow can be considered incompressible for Mach number lower than 0.3 [10]. In order to keep the Mach number below 0.3, we should determine the upper limit of Re. The following equation relating Mach number, Knudsen number and Reynolds number:

$$Re = \frac{Ma}{Kn}\sqrt{\frac{\pi\gamma}{2}} \quad (7)$$

By referring to Eq. (7) and the range of Knudsen number considered in this work, the flow will be incompressible with $\mathrm{Re} = 2$. Hence, all subsequent results presented were obtained using this Reynolds number.

Moreover, the other boundary conditions should be defined. Uniform inlet velocity and temperature distributions are specified as

$$u = 1, v = 0, \theta = 0 \quad (8)$$

In the outlet, fully developed boundary conditions are assumed as

$$\frac{\partial u}{\partial x} = \frac{\partial v}{\partial x} = \frac{\partial \theta}{\partial x} = 0 \quad (9)$$

4. Calculations for Nusselt number and C_f.Re

Friction coefficient for a hydrodynamically–thermally developing flow in the micro channel is calculated by,

$$C_f = \frac{\tau_w^*(x)}{\rho\left(u_{ave}^*(x)\right)^2} \tag{10}$$

where $u_{ave}^*(x)$ represents the average velocity and $\tau_W^*(x)$ is the wall shear stress. Eq. (10) can be expressed in non-dimensional form as

$$C_f Re = \frac{4(y(x))^2}{\left(\int u(x,y)\,dy\right)^2}\frac{\partial u^{tang}(x)}{\partial n} \tag{11}$$

The local Nusselt number is calculated by

$$Nu = \frac{hL^*}{k} \tag{12}$$

Eq(12) can be expressed in non-dimensional form as

$$Nu = \frac{1}{\theta_{ave}(x)-1}\frac{\partial\theta(x)}{\partial n}\bigg|_w \tag{13}$$

5. Validation of numerical code

In Fig. 2, a comparison with the previously published result of Wang and Chen [4] is done to validate the numerical code and non-orthogonal grid discretization scheme of the present study. Their model is analogous to the present model but with the water as working fluid and macro scale channel. There is no slip effect with fixing Knudsen number at zero.

6. Grid dependence

The accuracy of the numerical solutions and the time required to reach a steady-state solution are dependent on the grid resolution. To clarify effect of mesh refinement on numerical solution, three meshes are used in numerical analysis: 550×65, 600×75 and 650×85. As it shows in Fig. 3, increasing the grid numbers does not significantly change in the surface Nusselt number. For Kn = 0.075 at Re = 2, 600×75 grid seems to be optimum in accuracy and run-time. Furthermore, similar type of grid independence study is carried out for the other Knudsen and Re numbers (not reported here) and optimum meshes are chosen.

7. Solution procedure

The governing equations with appropriate boundary conditions are solved by employing the SIMPLE algorithm [13], a finite-volume method, in non-orthogonal curvilinear coordinate framework. A fully implicit scheme is used for the temporal terms and the HYBRID differencing [14] is applied for the approximation of the convective terms. The Poisson equations is solved for (x, y) to find grid points [15] and are distributed in a non-uniform manner with higher concentration of grids close to the curvy walls and normal to all walls, as shown in Fig. 1. In this work, a full-staggered grid is used. The discrete form of the momentum and energy equations and all the boundary conditions are obtained by applying a second order central difference scheme.

One convergence criteria is a mass flux residual less than 10^{-8} for each control volume. Another criteria is $(|\varphi_{i+1}-\varphi_i|)/|\varphi_{i+1}|\leq 10^{-10}$ where φ represents any dependent variable, namely u, v and θ, and i is the number of iteration.

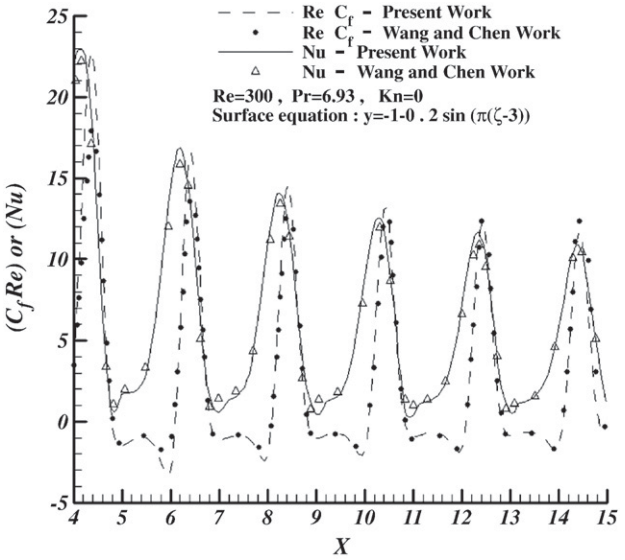

Fig. 2. Validation of the numerical code with available results.

8. Results and discussion

In order to have a physical point of view of the problem and for the purpose of calculating the fluid flow and heat transfer characteristics, numerical calculations are carried out, for different values Knudsen number and various amplitude values. Because of the symmetrical geometry, in this work, only one half of microchannel is numerically solved. Therefore, the time of computation work reduces considerably. However, the results depicted for the whole microchannel. The tangential momentum accommodation coefficient σ_v and the thermal accommodation coefficient σ_T are set at 0.9. In this work, the Eckert Number is not constant. With defined Re and Knudsen number and using Eq. (7) the Mach number is calculated. Now with the calculated Mach number and using Eq. (14), one can compute the inlet velocity. The obtained inlet velocity and Eq. (6) result in the Eckert number.

$$u_i^* = Ma\sqrt{\gamma RT_i} \tag{14}$$

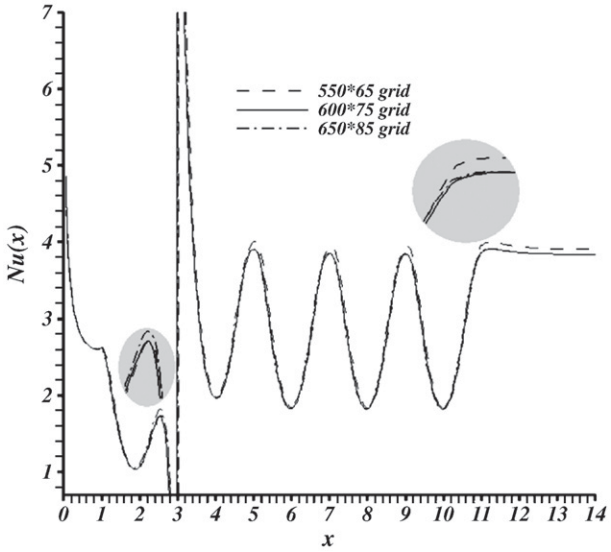

Fig. 3. Numerical results of local Nusselt number along the wavy microchannel with Kn = 0.075 at Re = 2.

Table 1
Numerical values for Ec as a function of Kn with Re = 2.

	Kn = 0.01	Kn = 0.025	Kn = 0.05	Kn = 0.075	Kn = 0.1
Ma	1.34×10^{-2}	3.37×10^{-2}	6.74×10^{-2}	0.1	0.13
Ec	4.82×10^{-4}	3.01×10^{-3}	1.21×10^{-2}	2.7×10^{-2}	4.82×10^{-2}

Furthermore, the boundaries are maintained at temperature $T_w = 70$ °C and the uniform inlet temperature is considered $T_i = 25$ °C. The results are obtained for the specific heat ratio $\gamma = 1.4$, Pr = 0.7 and $\lambda = 2$. The data on Table 1 shows the five studied Knudsen numbers and corresponding Mach number and Eckert number.

8.1. The flow field

Fig. 4 shows the effect of Knudsen number on slip velocity for hydrodynamically/thermally developing flow in the wavy microchannel. By increasing the Knudsen number, the channel dimensions decrease and approach to molecular dimensions. By decreasing the microchannel dimensions, the MFP (mean free path) becomes more comparable with the microchannel's characteristic length in size. This means that the thickness of Knudsen layer increases that causes an increase in the slip velocity. Moreover, in the convergent region, the cross section area decreases that causes the acceleration of the fluid flow. So the average velocity increases that contributes to a rapid raise in the slip velocity in this region. In the divergent area, contrary to the convergent area, the cross section area increases. This increase causes a rapid decline in the slip velocity as it can be observed.

Fig. 5 illustrates the velocity profiles. As it can be observed by increasing the rarefaction, the slip flow is intensified and the slip velocity value becomes greater. The data in this figure illustrates that as slip velocity increases, the velocity profile gets flattered that leads to the reduction in wall velocity gradients.

Fig. 6 compares the velocity profile in different Knudsen numbers and in different cross sections. It schematically shows when rarefaction increases, the slip velocity values become greater. In addition, in each Knudsen number as the fluid approached throttle regions, the slip velocity becomes more considerable.

Fig. 7 depicts C_f.Re versus Knudsen number for hydrodynamically/thermally developing flow in the wavy microchannel. It is evident that there is high friction at the entrance region due to presence of high velocity gradients. However, it rapidly decreases as the flow develops.

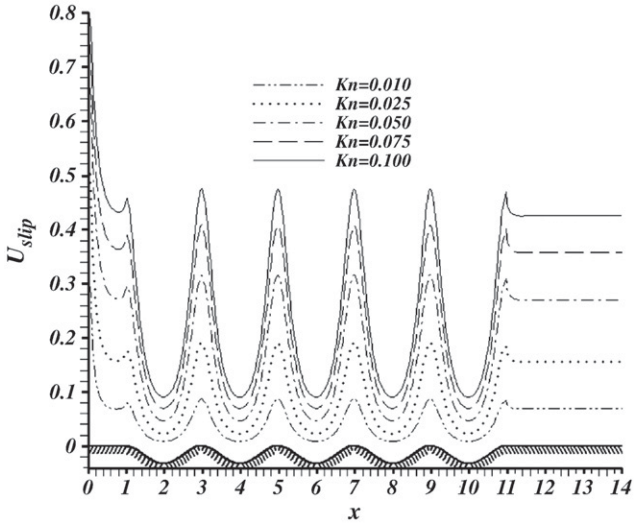

Fig. 4. Variation of slip velocity along the wavy microchannel with Knudsen number Re = 2 and $a = 2$.

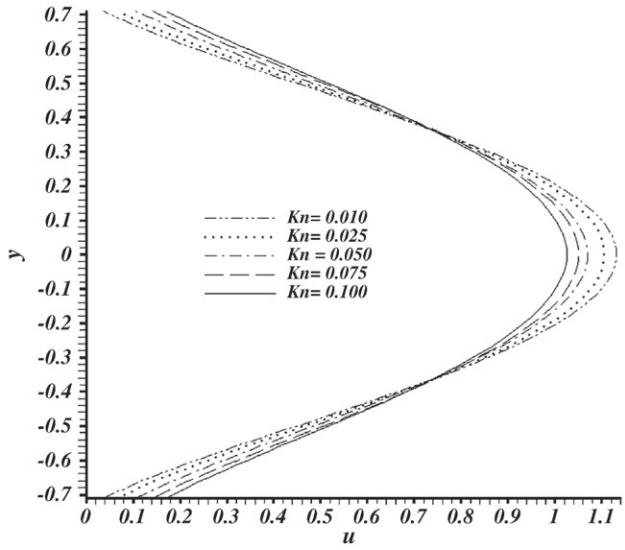

Fig. 5. Variation of velocity profile at $x = 0.75\lambda$ the wavy microchannel with Knudsen at Re = 2 and $a = 2$.

Moreover, rarefaction has a decreasing effect on the friction factor. For instance, by variation of Knudsen number from 0.01 to 0.1, the C_f.Re at the end of micro channels decreases 37%. This effect can be explained physically. By increasing the Knudsen number, as already stated, the interaction of gaseous molecules with the adjacent walls decreases. Therefore, the momentum exchange between the fluid and adjacent walls reduces and this means C_f.Re declines. Furthermore, as rarefaction increases, the slip velocity increases which results in a flatter velocity profile that reduces wall velocity gradients and contributes to the decrease in C_f.Re. However, this effect can be interpreted mathematically. Eq. (11) shows that C_f.Re depends on the

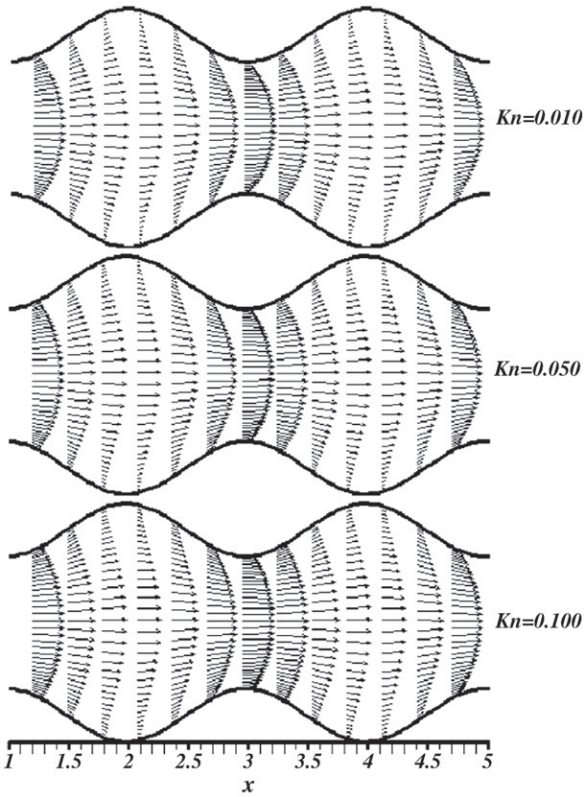

Fig. 6. Schematic illustration of Knudsen effect on velocity profile at Re = 2 and $a = 2$.

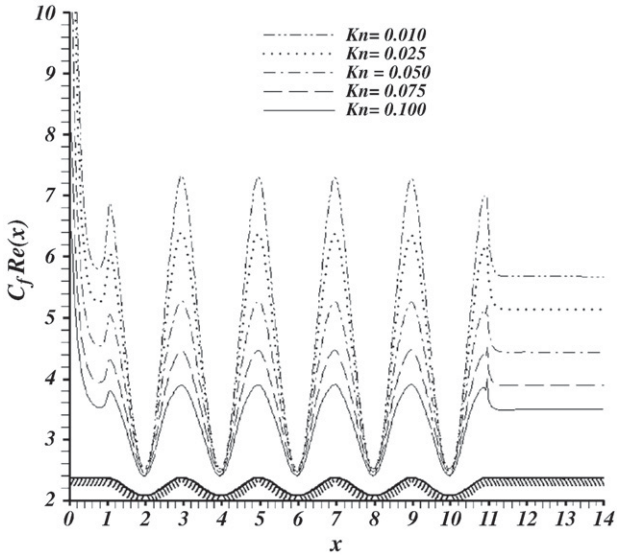

Fig. 7. Variation of C_f.Re along the wavy microchannel with Knudsen at Re = 2 and $a = 2$.

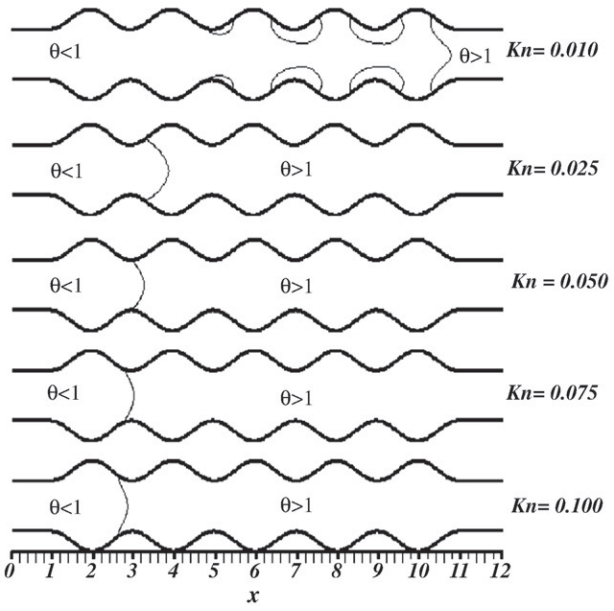

Fig. 8. Isothermal line corresponds to non-dimensional temperature unity along the wavy microchannel with Knudsen at Re = 2 and $a = 2$.

average velocity and the gradient of tangential velocity. As Knudsen increases, due to a fixed Re and Eq. (7), the Mach number increases that results in greater average velocity. In addition, in according to Fig. 5, larger Knudsen number decreases the slop of velocity near the wall and this means having lesser tangential velocity gradient. Therefore, in according to the previous explanation, the larger Knudsen number causes the lesser C_f.Re.

As it can be observed in Fig. 7, when the fluid flows in the divergent region, C_f.Re experiences a rapid decrease in the microchannel. To explain this phenomenon, one should refer to the definition of C_f.Re in Eq. (11). In this equation, there are three different parameters that should be considered separately. The first parameter is the gradient of tangential velocity, $\partial u^{tang}(x)/\partial n$ that reduces in the divergent area because of reduction of the average velocity through this area. The second term is the inverse of square of average velocity that decreases in the divergent area. The third term is the square of channel width cross four, $4y(x)^2$ that increases through the divergent area. The behavior of C_f.Re is determined by summing of these three terms. In this case, intensity of variation of $\partial u^{tang}(x)/\partial n$ is more significant and determines the behavior of C_f.Re.

8.2. The temperature field

Fig. 8 displays the isothermal line corresponds to the non-dimensional temperature of unity for five different values of Knudsen number. Two different thermal regions can be distinguished inside the channel, namely the region of $\theta<1$ and $\theta>1$. In the inlet of channel, the non-dimensional temperature is less than unity. When the fluid flows through the channel, its temperature increases due to the heat supplied by the wall into the fluid. In the region close to $\theta = 1$, the heat supplied by the wall into the fluid is balanced by the internal heat generation due to the viscous heating. In the region of $\theta>1$, the internally generated heat by the viscous dissipation overcomes the wall heat. As it can be observed the effect of viscous dissipation is an important effect in microchannels. By increasing Knudsen number, this effect can be more important.

The effect of Knudsen number on temperature jump is depicted in Fig. 9. As shown, larger Knudsen numbers leads to higher temperature jumps. By decreasing of the channel dimensions, the thickness of the Knudsen layer increases that brings about further temperature jumps. This increase has two different directions though. In the inlet of microchannel, the fluid temperature near the wall is less than the wall temperature. In this region, when the temperature jump is raised, the fluid temperature near the wall tends to become less than the wall temperature (i.e., towards the inlet temperature). In the outlet of microchannel, the fluid temperature near the wall is more than the wall temperature. In this region, the fluid temperature near the wall tends to become higher than the wall temperature (i.e., contrary to the inlet temperature) when the temperature jump is raised by increasing Knudsen number. It is further noticed that with an increase in Knudsen number, the effect of viscous dissipation becomes more important. For instance, in Kn = 0.1, the fully developed non-dimensional fluid temperature near the wall is larger than 1.01. In addition, it is found that the fluid temperature near the wall increases along the microchannel generally. However this effect is gradually diminishing as the fluid flow approaches the developed region.

Fig. 10 illustrates the variation of average temperature versus the length of microchannel for different Knudsen numbers. In the entrance of microchannel, by increasing rarefaction, the average

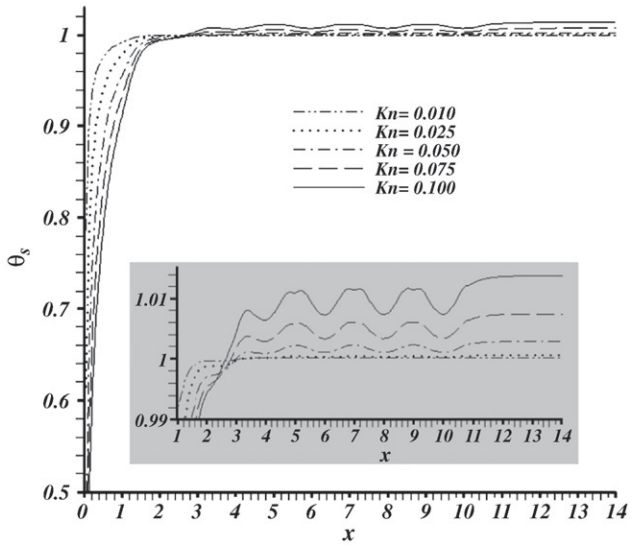

Fig. 9. Variation of slip temperature with Knudsen number along the wavy microchannel at Re = 2 and $a = 2$.

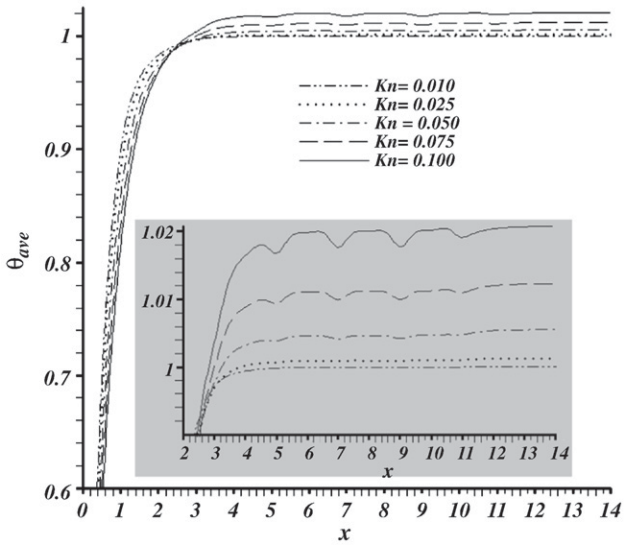

Fig. 10. Variation of average temperature with Knudsen number along the wavy microchannel with Re = 2 and $a = 2$.

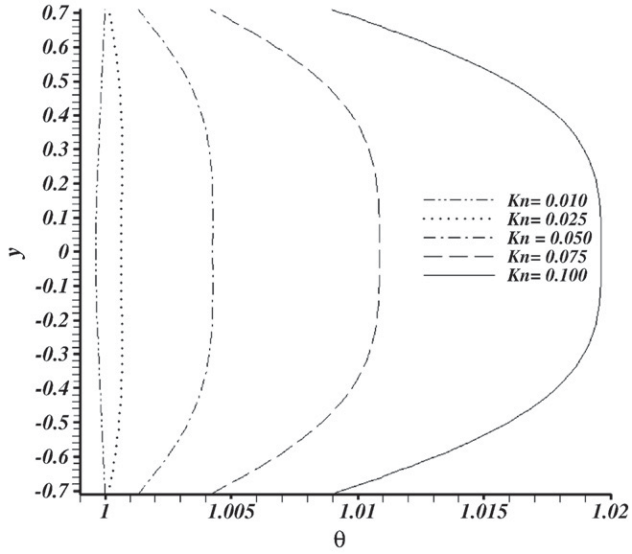

Fig. 12. Variation of temperature profile at $x = 2.25\lambda$ in the wavy microchannel with Knudsen at Re = 2 and $a = 2$.

temperature decreases. When Knudsen number increases, the inlet velocity increases. As the fluid enters with greater momentum, it loses its chance to exchange energy with the adjacent walls. It leads to decrease in the average temperature. However, when the fluid flows along the microchannel, the effect of viscous dissipation becomes more important. Viscous dissipation effect is closely related to the fluid velocity. By increasing Knudsen number, the fluid velocity increases and causes more viscous dissipation effect and consequently higher average temperature. It can be also noticed that by increasing Knudsen number, the axial distance from the channel entrance to the fully developed region, gets longer.

Fig. 11 and Fig. 12 present temperature distributions in two different cross sections at $x = 0.75\lambda$, 2.25λ. In Fig. 11, all profiles are plotted in the region $\theta < 1$. As expected with larger Knudsen number, higher temperature jump at the wall is present. In according to the definition, a unity non-dimensional temperature means the temperature of the fluid equals wall temperature. Intensification of Knudsen number causes the center non-dimensional temperature to approach the inlet non-dimensional temperature more. Also in this region, all tangential temperature gradients are negative.

In Fig. 12, profiles correspond to Kn = 0.025, 0.05, 0.075 and 0.1 are plotted in the region $\theta > 1$.

In this region, the fluid temperature near the wall tends to become higher than the wall temperature (i.e., contrary to the inlet temperature) when the temperature jump is raised by increasing Knudsen number. Also in this region, all tangential temperature gradients are positive and are intensified by increasing Knudsen number.

Fig. 13 presents the variation of local Nusselt number with the microchannel length using different Knudsen numbers. As expected, very high heat transfer rates are experienced in the entrance region of the microchannel due to high temperature gradient. As expected also, high heat transfer rates diminish rapidly as the thermally developing flow approaches the fully developed flow.

As it can be observed, there is a singular point for each Knudsen number in Nusselt profile. The physical reason of the singularity is the

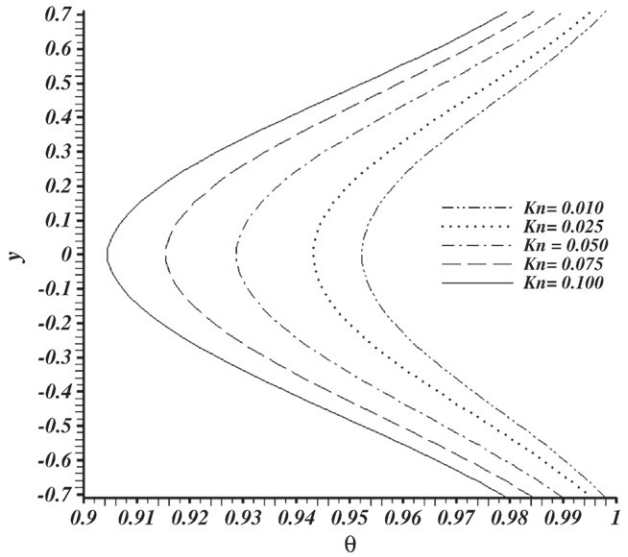

Fig. 11. Variation of temperature profile at $x = 0.75\lambda$ in the wavy microchannel with Knudsen at Re = 2 and $a = 2$.

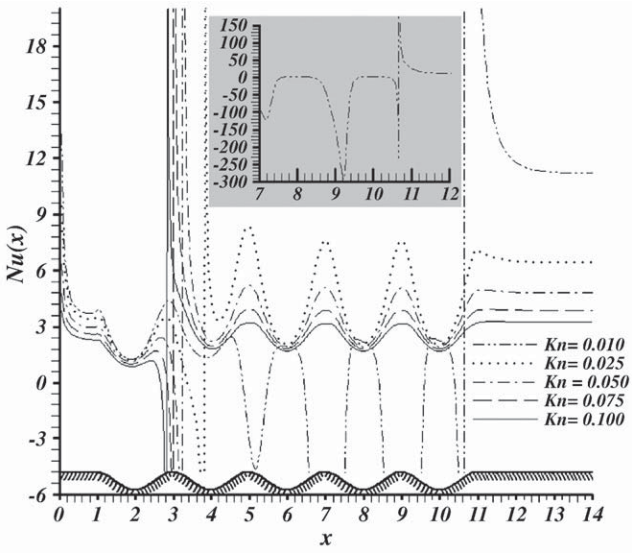

Fig. 13. Variation of local Nusselt along the wavy microchannel with Knudsen at Re = 2 and $a = 2$.

presence of an axial position where the difference between the average temperature and wall temperature vanishes. Actually, in the singular point, the heat supplied by the wall into the fluid is balanced by the internal heat generation due to the viscous heating. With the increasing Knudsen number, this critical point is reached at an earlier point from the entrance. This displacement is originated by the viscous dissipation effect. As it can be noticed from Fig. 8, the effect of viscous dissipation becomes more significant and the region $\theta>1$ grows by increasing Knudsen number.

In the region $\theta<1$, the average non-dimensional temperature is less than the wall temperature. Also according to Fig. 11, the tangential temperature gradient is negative in this region. Therefore, Nusselt number is positive in accord with Eq. (13). The average non-dimensional temperature is more than the wall temperature and the tangential temperature gradient is positive in the region $\theta>1$. So, Nusselt number is positive in this region for each Knudsen number. The trend of Nusselt profile related to Kn = 0.01 is different though. As it can be seen, Nusselt number is partially negative in region of $\theta<1$. This can be explained by referring to Fig. 8. As it can be noticed, there are some small regions that the fluid temperature near the wall is more than the wall temperature in $\theta<1$. So the average temperature and tangential temperature gradient are affected by these discrete regions.

Moreover, Nusselt number in the microchannel decreases as the rarefaction increases. For instance, by variation of Knudsen number from 0.01 to 0.1, the Nusselt number at the end of micro channels decreases 71%. As already sated, when rarefaction increases the temperature jump as well as slip velocity is intensified. Here, as temperature jump intensifies, the absolute difference between the average temperature and wall temperature becomes more. The temperature jump acts like a thermal contact resistance between the wall and gas. However, the slip velocity tends to decrease this thermal resistance. In other words, the effects of the temperature jump and slip velocity are opposite on Nusselt number. The slip velocity acts to increase the Nusselt number by increasing the fluid velocity near the wall. Contrary to the slip velocity, the temperature jump decreases the Nusselt number by increasing the absolute difference of the wall temperature and mean gas temperature. In this work, with $\sigma_v = 0.9$, $\sigma_T = 0.9$ and the specified geometry, the effect of temperature jump in Nusselt number is more important.

In addition, due to the increasing of the average velocity and especially slip velocity in the convergent region, there is a jump in the local Nusselt in this region and this amplifies the heat transfer coefficient. There is the same phenomenon in macro scale channel because of larger average velocity in converging region. As the fluid flow approaches the developed region, local Nusselt number converges to a constant value (i.e., there is no change in local Nusselt).

9. Conclusion

Developing fluid flow and heat transfer through a wavy micro-channel have been studied by taking the effect of viscous dissipation into account. The present work investigates the effects of Knudsen number and geometry on thermal and hydrodynamic characteristics of flow in the wavy microchannel at constant Reynolds number.

It is found that the Nusselt number and C_f.Re decrease with Knudsen number. It is also found, in the divergent parts, Nusselt number experiences a rapid decrease. In addition, the very high heat transfer rate and C_f.Re at the entrance declines rapidly as the thermally-hydraulically developing flow approaches fully developed flow. Moreover, the model successfully predicts the growth of temperature jump and slip velocity with Knudsen number at the solid walls.

Furthermore, it is observed that the effect of viscous dissipation has a considerable effect in microchannels. This effect can be more significant by increasing Knudsen number. Also, it leads a singular point in Nusselt profiles.

References

[1] L. Biswal, S.K. Som, S. Chakraborty, Effects of entrance region transport processes on free convection slip flow in vertical microchannels with isothermally heated walls, International Journal of Heat and Mass Transfer 50 (2007) 1248–1254.
[2] G. Hetsroni, A. Mosyak, E. Pogrebnyak, L.P. Yarin, Fluid flow in micro-channels, International Journal of Heat & Mass Transfer 48 (2005) 1982–1998.
[3] A. Beskok, G.E. Karniadakis, Simulation of heat and momentum transfer in complex microgeometries, Journal of Thermophysics and Heat Transfer 8 (1994) 647–655.
[4] C.-C. Wang, C.-K. Chen, Forced convection in a wavy-wall channel, International Journal of Heat and Mass Transfer 47 (2004) 3877–3887.
[5] J.E. O'Brien, E.M. Sparrow, Corrugated-duct heat transfer, pressure drop, and flow visualization, Journal of Heat Transfer 104 (1982) 410–416.
[6] E.B. Arkilic, K.S. Breuer, M.A. Schmidt, Gaseous flow in microchannels, ASME Application of Microfabrication to Fluid Mechanics 197 (1994) 57–66.
[7] A. Beskok, G.E. Karniadakis, W. Trimmer, Rarefaction and compressibility effects in gas microflows, Journal of Fluids Engineering Transactions of the ASME 118 (3) (1996) 448–456.
[8] L. Kuddusi, E. Çetegen, Thermal and hydrodyna-mic analysis of gaseous flow in trapezoidal silicon microchannels, International Journal of Thermal Sciences 48 (2009) 353–362.
[9] Cha'o-Kuang Chen, Ching-Chang Cho, Electro-kinetically-driven flow mixing in microchannels with wavy surface, Journal of Colloid and Interface Science 312 (2007) 470–480.
[10] G.E. Karniadakis, A. Beskok, N. Aluru, Micro Flows and Nanoflows, Fundamental and Simulation, Springer, USA, 2004.
[11] S. Kandlikar, S. Garimella, D. Li, S. Colin, M.R. King, Heat Transfer And Fluid Flow in Minichannels and Microchannels, Elsevier, Britain, 2006.
[12] W.W. Liou, Y. Fang, Microfluid Mechanics, Principal and Modeling, McGraw-Hill, New York, 2006.
[13] S.V. Patankar, A calculation procedure for heat, mass and momentum transfer in three-dimensional parabolic flows, International Journal of Heat Mass Transf 15 (1972) 1787–1806.
[14] D.B. Spalding, A novel finite difference formulation for differential expressions involving both first and second derivatives, International Journal for Numerical Methods in Engineering 4 (1972) 551–559.
[15] K.A. Hoffman, Computational Fluid Dynamics for Engineers, Engineering Education System, Austin, 1989.